



The facile synthesis of hierarchical NiCoO₂ nanotubes comprised ultrathin nanosheets for supercapacitors



Xin Xu^a, Han Zhou^a, Shujiang Ding^{a,*}, Jun Li^b, Beibei Li^b, Demei Yu^{a,*}

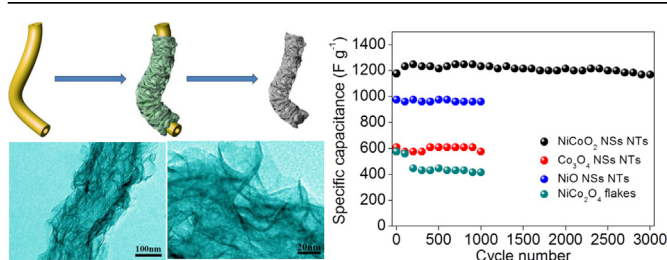
^a Department of Applied Chemistry, School of Science and MOE Key Laboratory for Nonequilibrium Synthesis and Modulation of Condensed Matter and State Key Laboratory for Mechanical Behavior of Materials, Xi'an Jiaotong University, Xi'an 710049, China

^b The Center of Nanomaterials for Renewable Energy, Xi'an Jiaotong University, Xi'an 710049, China

HIGHLIGHTS

- NiCoO₂ nanosheets nanotubes are prepared against polymeric nanotube template.
- The products show superior specific capacitance and cycling stability.
- The smart nanostructures are favorable for fast ion and electron transfer.

GRAPHICAL ABSTRACT



ARTICLE INFO

Article history:

Received 14 February 2014

Received in revised form

14 May 2014

Accepted 14 May 2014

Available online 29 May 2014

Keywords:

Nickel cobaltite

Nanosheets

Nanotubes

Supercapacitor

ABSTRACT

Hierarchical NiCoO₂ nanosheets nanotubes are successfully prepared by a mild solution method based on the template of polymeric nanotubes (PNT) followed by a thermal annealing treatment. The microstructure and chemical composition of NiCoO₂ nanosheets nanotubes are characterized by scanning electron microscopy (SEM), transmission electron microscopy (TEM), Brunauer–Emmett–Teller (BET) analyzer, X-ray diffraction (XRD) and Thermogravimetric analysis (TGA). When evaluated as an electrode material for supercapacitors, the results of electrochemical test show that the unique NiCoO₂ nanosheets nanotubes exhibit relatively high specific capacitance of 1468, 1352, 1233, 1178, 1020 and 672 F g^{−1} at the discharge current densities of 2, 4, 8, 10, 20 and 40 A g^{−1}, respectively. They also reveal an excellent cycling stability of 99.2% retention after 3000 cycles at 10 A g^{−1}. The smart nanostructures of the NiCoO₂ nanosheets nanotubes make a prominent contribution to the excellent electrochemical performance.

© 2014 Elsevier B.V. All rights reserved.

1. Introduction

The ever-increasing energy demand has greatly stimulated extensive research on high performance electrode materials for energy-storage devices, such as consumer electronic devices and electric vehicles [1]. Supercapacitors, have been considered as a kind of pivotal electric energy storage device because of their

higher power density, faster charge/discharge process, and longer working lifetime together with Lithium-ion batteries (LIBs) [2–5]. Unfortunately, the existing electrode materials are less satisfactory: the low specific capacitance for carbon-based materials, the poor cycling stability for pseudocapacitive materials and the high cost for RuO₂ based materials. Due to the difficulties on raising the specific capacitance of carbon-based materials, more attention is focused on the pseudocapacitive materials to enhance their cycling stability. Recently, the development of nanostructured materials, especially metal oxides, will indisputably provide a promising solution to solve the above-mentioned problems on account of the increased active surface areas and short ion transport pathways

* Corresponding authors.

E-mail addresses: dingsj@mail.xjtu.edu.cn (S. Ding), dmyu@mail.xjtu.edu.cn (D. Yu).

[6–8]. Among various nanostructures, mesoporous, hollow and hierarchical nanomaterials have been demonstrated as prospective candidates for energy storage, in view of their high surface area, capability of alleviating the volume change during the charge/discharge process, and their increased electroactive sites [9–12]. Therefore, it will be of great significance to develop efficient and simple routes to fabricate some kinds of electroactive materials with mesoporous, hollow and hierarchical nanostructures for supercapacitors.

Mixed transition metal oxides, typically ternary metal oxides with two different metal cations, have received numerous interests recently on account of their promising roles in many energy-related fields, such as lithium-ion batteries, supercapacitors, metal–air batteries, and fuel cells [13–15]. Recently, ternary nickel cobaltite has been widely investigated as a high-performance electrode material for energy storage (including lithium-ion batteries and supercapacitors) due to its low cost, environmentally benign nature, natural abundance and high theoretical capacitance. Moreover, ternary nickel cobaltite possesses much better electrical conductivity and higher redox activity compared to nickel oxide and cobalt oxide, which originate from the co-existence of the Ni and Co species [13,16–21]. Therefore, synthesizing ternary nickel cobaltite with a rationally designed morphology and nanoscale structure provides one of the most practicable methods to create high-performance supercapacitors. To date, there have been several reports on the synthesis and electrochemical evaluation of nanostructured NiCo_2O_4 materials such as nanosheets [13], nanoparticles [16], nanowires [17,18], and nanoflowers [21]. In addition, the Ni^{2+} could not only replace Co^{2+} in the spinel Co_3O_4 to form the NiCo_2O_4 , but also in the NaCl-type crystal CoO structure and thus forming the cubic NiCo_2O_4 . On the other hand, Co^{2+} and Ni^{2+} could co-exist in any molar ratio in the NaCl-type crystal structure, leading to the possible formation of $\text{Co}_x\text{Ni}_{1-x}\text{O}$ crystals. Yang and co-workers reported that when the molar ratio of Co^{2+} and Ni^{2+} is 1:1, the $\text{Co}_x\text{Ni}_{1-x}\text{O}$ products possess the best electrochemical performance [22].

In this work, we use polymeric nanotubes (PNTs) with uniform size as hard templates for preparation of NiCo_2O_4 nanosheets nanotubes, which is synthesized by cationic polymerization of divinylbenzene using immiscible initiator nanodroplets of boron trifluoride etherate complex and followed a sulfonation process [23]. Then we fabricate the NiCo_2O_4 nanosheets nanotubes by a simple and economical solution route with the synthetic process illustrated in Scheme 1. Firstly, we prefabricate NiCo-precursor@PNT based on in situ growth of NiCo-precursor ultra-thin nanosheets from the sulfonated gel matrix of polymeric nanotubes. After being calcined in air, the well-developed mesoporous and hierarchical NiCo_2O_4 nanosheets nanotubes are successfully obtained. The as-obtained NiCo_2O_4 nanosheets nanotubes are believed to be very suitable as the electrode material for

supercapacitors for at least three reasons: firstly, the higher specific surface area of these NiCo_2O_4 nanosheets nanotubes can provide more sites for redox reaction between the active materials and electrolyte ions, leading to outstanding rate performance and specific capacity. Secondly, massive void spaces derived from cavity and piling up nanosheets could effectively buffer the strain generated during the fast charging/discharging process, hence improving the cycling performance. Lastly, the two ends of the nanotubes are totally open, providing additional paths for ions in solution.

2. Experimental section

2.1. Materials synthesis

2.1.1. Synthesis of sulfonated PNTs

PNTs were prepared according to a previously reported method [23]. PNTs (3 g) were added to concentrated sulfuric acid ($\text{PNTs}:\text{H}_2\text{SO}_4 = 1:30$, w/w) and the mixture was ultrasonicated for 10 min to ensure well dispersion. After being stirred for 24 h at 40 °C, the red precipitate was collected by centrifugation and washed thoroughly with ethanol [24–26].

2.1.2. Synthesis of NiCo-precursor@PNT

75 mg $\text{Ni}(\text{NO}_3)_2 \cdot 6\text{H}_2\text{O}$, 150 mg $\text{Co}(\text{NO}_3)_2 \cdot 6\text{H}_2\text{O}$ and 35 mg hexamethylenetetramine (HMT) were dissolved into 40 mL 0.7 mM trisodium citrate solution. Then 15 mg sulfonated PNTs were dispersed into the above solution by sonication for 10 min. The reaction mixture was transferred into a 100 mL round bottom flask. After stirring for 6 h at 90 °C, the flask was left to cool down to room temperature. The precipitate was collected by centrifugation, washed thoroughly with ethanol, and dried at 60 °C overnight.

2.1.3. Synthesis of NiCo_2O_4 nanosheets nanotubes

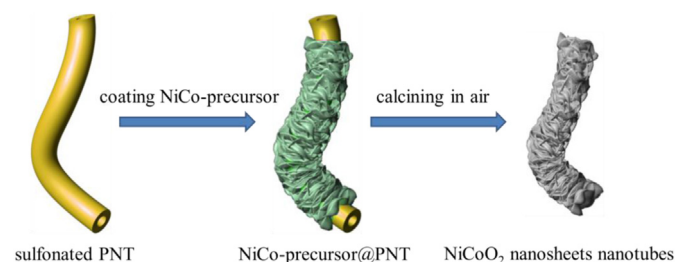
To obtain the NiCo_2O_4 nanosheets nanotubes, the as-prepared NiCo-precursor@PNT composite was subjected to calcination at 400 °C for 2 h to remove the PNTs templates and obtain the product.

The NiO and Co_3O_4 nanosheets nanotubes were prepared by adding only $\text{Ni}(\text{NO}_3)_2 \cdot 6\text{H}_2\text{O}$ or $\text{Co}(\text{NO}_3)_2 \cdot 6\text{H}_2\text{O}$ to the reaction system and through a similar following process.

The NiCo_2O_4 flakes were prepared by a similar method without PNTs.

2.2. Characterization

The product morphology was examined using field-emission scanning electron microscopy (FESEM; JEOL, JSM-7000F) and transmission electron microscopy (TEM; JEOL, JEM-2100). Crystallographic information of the samples was collected using powder X-ray diffraction (XRD; SHIMADZU, Lab X XRD-6000). Thermogravimetric analysis (METTLER-TOLEDO TGA 1) was carried out under a flow of air with a temperature ramp of 10 °C min^{-1} from room temperature to 600 °C. The specific surface area and pore size distribution of the products were measured using a BET analyzer (Autosorb-iQ, Quantachrome Instruments U.S.) at 77 K. The chemical states of the products were studied using the X-ray photoelectron spectroscopy (XPS) measurement performed on an Axis Ultra, Kratos (UK) at monochromatic Al K α radiation (150 W, 15 kV and 1486.6 eV). The vacuum in the spectrometer was 10–9 Torr. Binding energies were calibrated relative to the C 1s peak (284.6 eV).



Scheme 1. Schematic illustration of the synthetic procedure of NiCo_2O_4 nanosheets nanotubes.

2.3. Electrochemical measurements

The working electrode was prepared by mixing 70 wt% of the active material (NiCoO₂ nanosheets nanotubes), 20 wt% of conducting agent (carbon black, super-P-Li), and 10 wt% of binder (polyvinylidene difluoride, PVDF, Aldrich). This mixture was then pressed onto the glassy carbon electrode (Aida Hengsheng Technology co. Ltd, Tianjin, China) and dried at 60 °C. The mass loading of the NiCoO₂ nanosheets nanotubes on glassy carbon electrode was 0.3–0.5 mg cm⁻². The electrolyte used was a 2 M KOH aqueous solution. The capacitive performance of the samples was tested on a CHI 660D electrochemical workstation with cyclic voltammetry and chronopotentiometry functions using a three-electrode cell where Pt foil serves as the counter electrode and a standard calomel electrode (SCE) as the reference electrode. When testing the cycling performance of NiCoO₂ nanosheets nanotubes, the beaker used to contain the KOH aqueous solution is covered by a plastic film to prevent the evaporation of water.

3. Results and discussion

Fig. 1 shows the SEM and TEM images of the PNTs templates and NiCo-precursor @PNT composite. As can be seen, the sulfonated PNTs templates reveal meandering and long morphology (Fig. 1A). From Fig. 1B and C, the bamboo-like tubular structure and smooth

surface can be clearly observed. Fig. 1D shows that almost every PNT is covered with NiCo-precursor ultrathin nanosheets, this may be attributed to the large amount of functional groups (–SO₃) uniformly distributed on the surface of the PNTs. As can be seen in Fig. 1E and F, large amount of uniform 1D nanostructures can be obtained with a hierarchical architecture compared to that of bare PNTs shown in Fig. 1A. These 1D nanostructures are composed of uniform and ultrathin nanosheets grown surrounding the surface of PNTs [27].

The microstructure and morphology of NiCoO₂ nanosheets nanotubes are investigated by SEM, TEM and HRTEM with the results shown in Fig. 2. Fig. 2A and B shows the SEM images of NiCoO₂ nanosheets nanotubes obtained after calcining the Ni-precursor@PNT composite at 400 °C for 2 h. It is distinctly that the obtained products maintain their tubular and sheets-like morphology, which could also benefit from the robust support of PNTs, as well as the slow heating rate applied during the annealing. From Fig. 2C and D we can see that the mesoporous NiCoO₂ nanosheets nanotubes possess hollow internal structure and hierarchical external construction, and the diameter of them is approximately 100 nm. In addition, the thickness of these ultrathin NiCoO₂ nanosheets is around 2–4 nm (Fig. 2E). The facts mentioned above determine that these superior NiCoO₂ nanosheets nanotubes are extremely suitable for supercapacitors. The HRTEM image (Fig. 2F) taken from the NiCoO₂ nanosheets nanotubes show

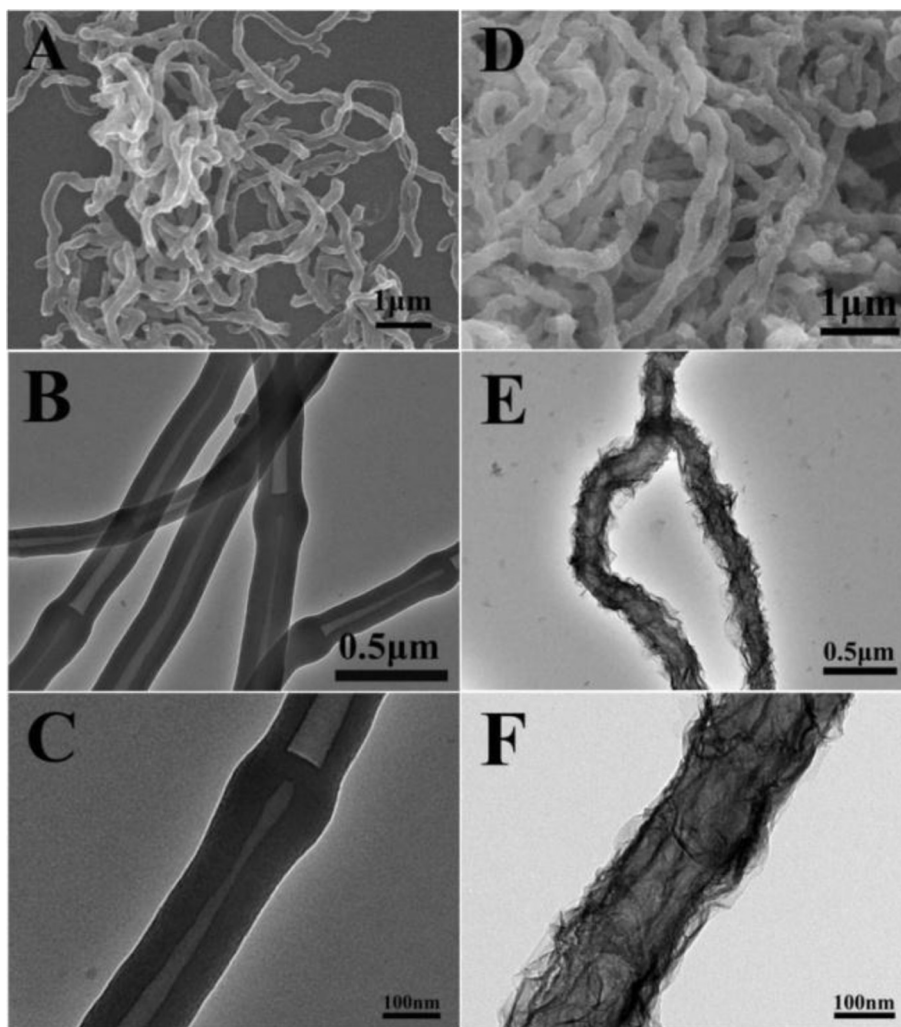


Fig. 1. (A) SEM image and (B, C) TEM images of the sulfonated PNTs templates; (D) SEM image and (E, F) TEM images of NiCo-precursor@PNT composite.

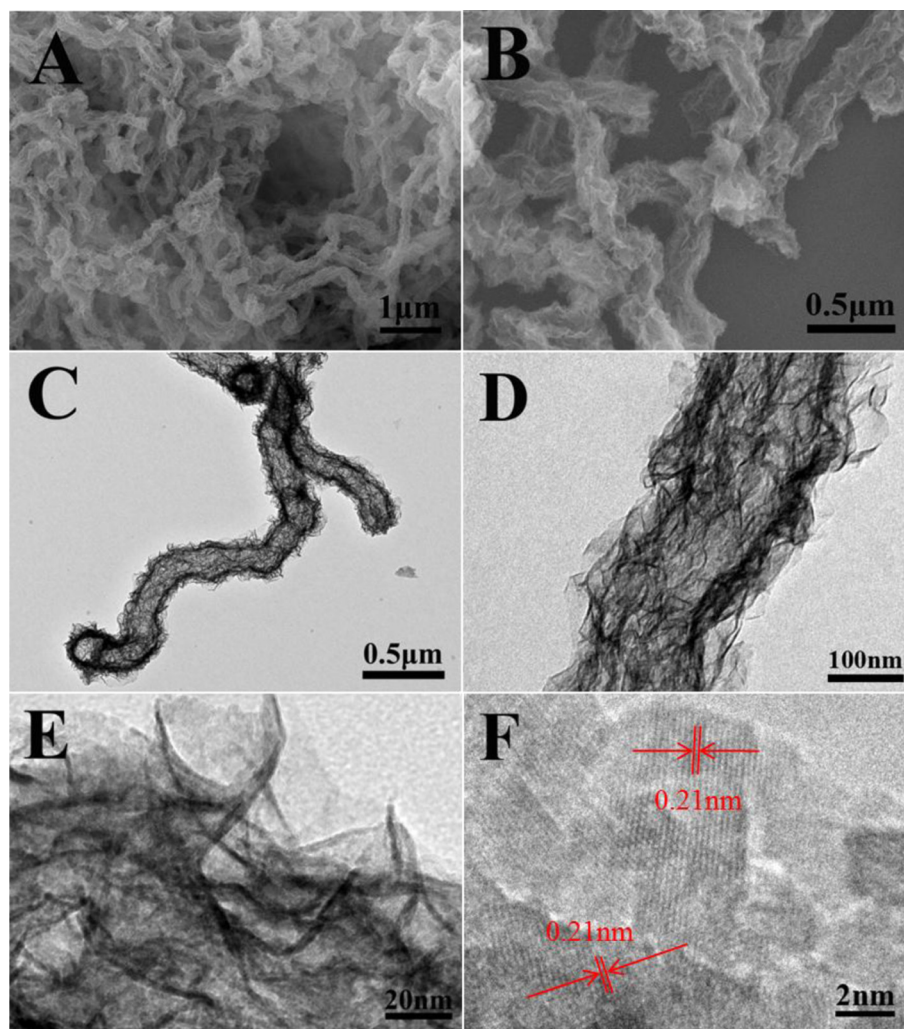


Fig. 2. SEM (A, B) images, TEM (C, D, E) images and HRTEM image (F) of hierarchical NiCoO₂ nanosheets nanotubes.

interplanar spacing of 0.21 nm, corresponding to that for the (200) facet of cubic structured NiCoO₂.

The resulting NiCoO₂ nanosheets nanotubes possess porous characteristic and large specific surface area, with the test results shown in Fig. 3. Nitrogen adsorption/desorption isotherm of the NiCoO₂ nanosheets nanotubes is shown in Fig. 3A, and the

corresponding Barrett–Joyner–Halenda (BJH) pore size distribution obtained from the desorption branch of the isotherm is shown in Fig. 3B. The Brunauer–Emmett–Teller (BET) specific surface area of NiCoO₂ nanosheets nanotubes is calculated to be 98.9 m² g^{−1}, and the size of the most pores which originate from the pile up of the nanosheets is in the range of 4–60 nm (Fig. 3B). The NLDFT

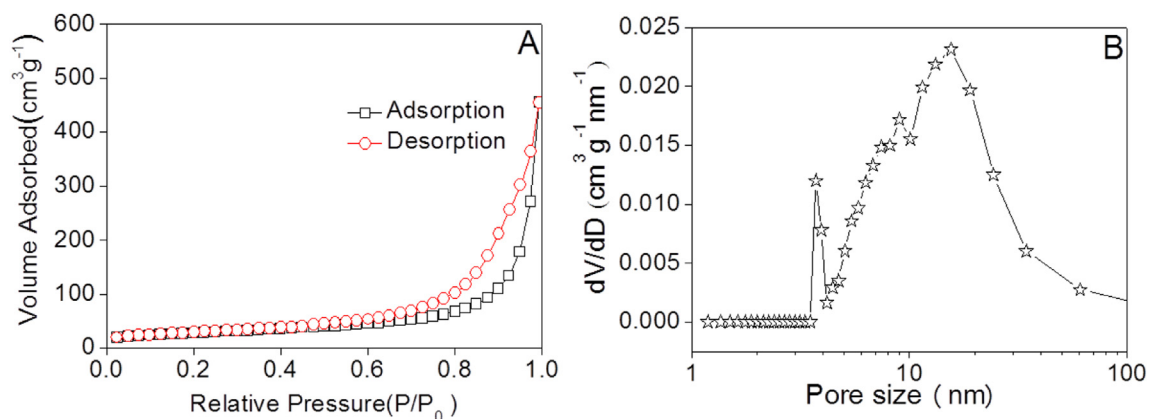


Fig. 3. (A) Nitrogen adsorption/desorption isotherm of the NiCoO₂ nanosheets nanotubes; (B) the pore size distribution calculated using the BJH method from the desorption curve.

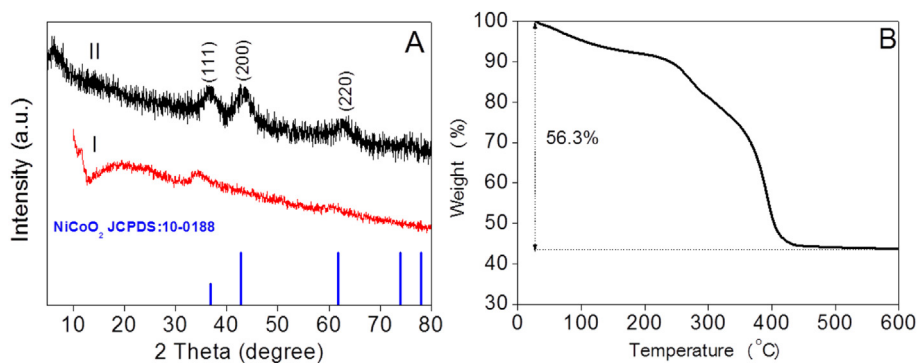


Fig. 4. (A) XRD patterns of NiCo-precursor@PNT composite (I) and NiCoO₂ nanosheets nanotubes (II); (B) TGA curve of the NiCo-precursor@PNT composite.

pore-size distribution of NiCoO₂ nanosheets nanotubes shows that the majority of the pores in the NiCoO₂ nanosheets nanotubes are in the range of 4–8 nm (Fig. S2).

Fig. 4A shows the corresponding XRD patterns of the NiCo-precursor@PNT composite and NiCoO₂ nanosheets nanotubes. As can be seen, The XRD pattern of NiCo-precursor nanosheets is

similar to that of the cobalt nickel carbonate hydroxide hydrate (JCPDS card no. 40-0216), while that of the annealed sample can be unambiguously assigned to the cubic NiCoO₂ phase (JCPDS card no. 10-0188). This result is also consistent with the HRTEM image. In addition, the X-ray photoelectron spectroscopy (XPS) measurements also confirmed the as-prepared products are NiCoO₂

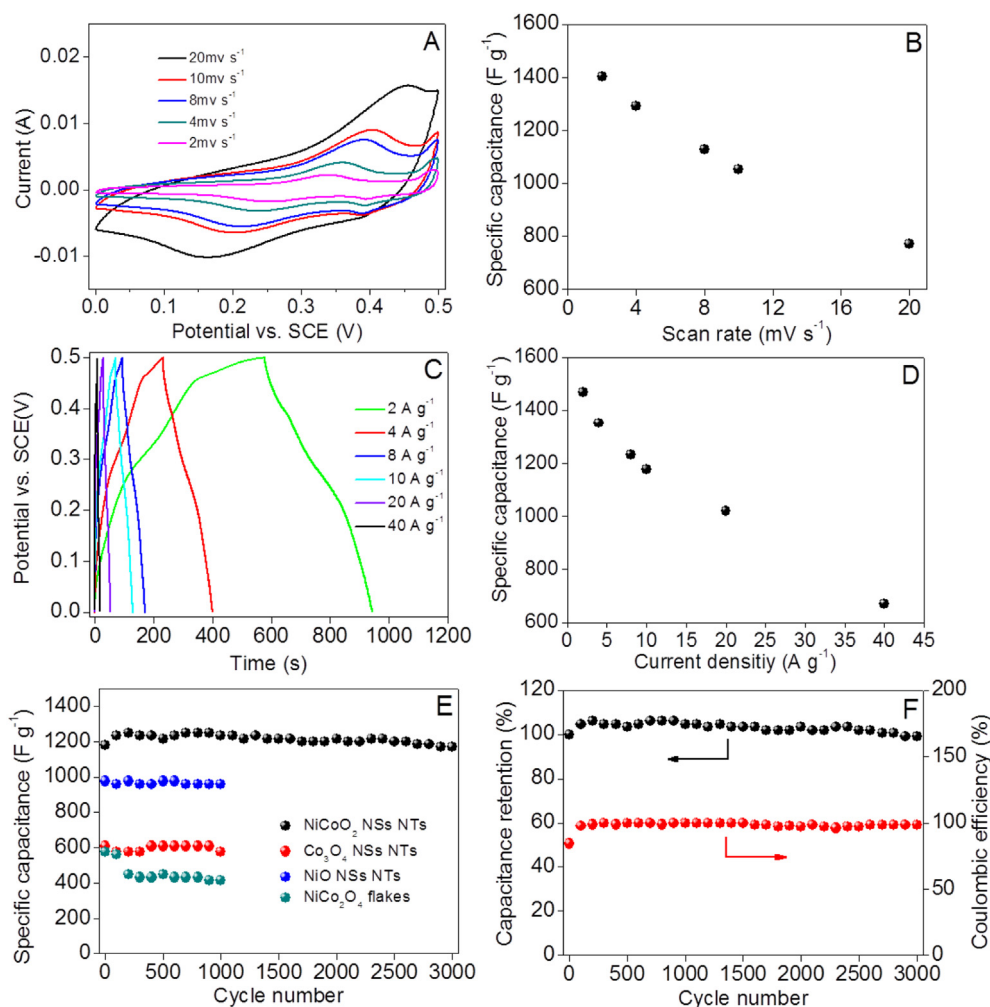


Fig. 5. Electrochemical characterizations of the NiCoO₂ nanosheets nanotubes. (A) CV curves at various scan rates ranging from 2 to 20 mV s⁻¹; (B) average specific capacitance of NiCoO₂ nanosheets nanotubes at various scan rates; (C) charge–discharge voltage profiles at various current densities ranging from 2 to 40 A g⁻¹; (D) average specific capacitance of NiCoO₂ nanosheets nanotubes at various discharge current densities; (E) average specific capacitance versus cycle number of NiCoO₂, NiO [34], Co₃O₄ nanosheets nanotubes and NiCo₂O₄ flakes at a current density of 10 A g⁻¹; (F) average specific capacitance retention and Coulombic efficiency versus cycle number of NiCoO₂ nanosheets nanotubes at a current density of 10 A g⁻¹.

nanosheets nanotubes (Fig. S3). The thermal behavior of NiCo-precursor@PNT was studied by TGA, with the results shown in Fig. 4B. The initial weight loss of NiCo-precursor@PNT below 360 °C can be mainly attributed to the removal of physically adsorbed water and partial decomposition of NiCo-precursor. When the temperature is above 360 °C, the decomposition of the sulfonated PNTs templates is beginning, thus we choose 400 °C to remove the PNTs templates. Finally, the curve flattens out at approximately 420 °C, indicating that the PNTs templates are totally removed and the NiCo-precursor is converted to NiCoO₂. After reaching 600 °C, the NiCo-precursor@PNT shows a total weight loss of 56.3%, the mass fraction of NiCoO₂ is about 43.7% in the NiCo-precursor@PNT nanostructure.

To prove the superiority of the NiCoO₂ nanosheets nanotubes, we subsequently investigate the electrochemical properties of the sample as an electrode for supercapacitors. Fig. 5A shows the typical cyclic voltammetry (CV) curves of the NiCoO₂ nanosheets nanotubes electrode with various scan rates ranging from 2 to 20 mV s⁻¹. The shape of the CV curves clearly reveals the pseudo-capacitive characteristics. Specifically, a pair of redox peaks can be observed within the potential range from 0 to 0.5 V vs. SCE for all sweep rates. The average specific capacitances of NiCoO₂ nanosheets nanotubes are calculated to be 1403, 1292, 1128, 1053 and 771 F g⁻¹ at scan rates of 2, 4, 8, 10 and 20 mV s⁻¹, respectively (Fig. 5B). Fig. 5C shows galvanostatic charge–discharge curves of the NiCoO₂ nanosheets nanotubes at different current densities ranging from 2 to 40 A g⁻¹. It is obviously that there is a plateau appears in every charge–discharge curve, corresponding to the CV measurement. The specific capacitance at different current densities can be calculated via Equation (1):

$$C_m = I \times \Delta t / (\Delta V \times m) \quad (1)$$

where C_m (F g⁻¹) is the specific capacitance, I (A) is the discharge current, Δt (s) is the discharge time, ΔV (V) is the potential change during discharge, and m (g) is the mass of the active material (NiCoO₂ nanosheets nanotubes) in each electrode. The calculated specific capacitance as a function of the discharge current density is plotted in Fig. 5D. Notably, the specific capacitance is as high as 1468, 1352, 1233, 1178, 1020, 672 F g⁻¹ at the discharge current densities of 2, 4, 8, 10, 20 and 40 A g⁻¹, respectively. It is worthy to be mentioned that the specific capacitance of our as-obtained NiCoO₂ nanosheets nanotubes is preferable compared with previously reported values of other NiCo₂O₄ based nanostructures [13,16,17,28–33]. In addition, the easy-to-make PNT templates make it possible to fabricate many other 1D metal oxide nanostructures in large-scale for energy storage. To make a further investigation, the cycling stability of NiCoO₂ nanosheets nanotubes is displayed in Fig. 5E at the discharge current density of 10 A g⁻¹, the specific capacitance is around 1178 F g⁻¹ in the first cycle, and it slightly increases to 1248 F g⁻¹ in the course of first two hundred cycles. After that, it gradually decreases to 1168 F g⁻¹ after 3000 cycles, resulting in an overall capacitance loss of only 0.8%. Furthermore, the Coulombic efficiency of the NiCoO₂ nanosheets nanotubes is nearly 100% during the whole cycles (Fig. 5F). As a comparison, we subsequently used NiO, [34] Co₃O₄ nanosheets nanotubes and NiCo₂O₄ flakes to investigate their cycling stability at the same current density of 10 A g⁻¹. As shown in Fig. 5E, the NiO and Co₃O₄ nanosheets nanotubes display relatively low specific capacitances of 960 and 576 F g⁻¹ after 1000 cycles, respectively. In addition, the NiCo₂O₄ flakes prepared without PNTs only reveal a specific capacitance of 416 F g⁻¹. The above-mentioned results reveal that these mesoporous and hierarchical NiCoO₂ nanosheets nanotubes have oppositely high supercapacitances and excellent cycling stability due to their outstanding 1D nanostructure.

4. Conclusions

In summary, we have developed a facile method to produce NiCoO₂ nanosheets nanotubes using sulfonated polymeric nanotubes as templates. When these unique NiCoO₂ nanosheets nanotubes were investigated as an electrode for supercapacitors, a high capacitance of 1168 F g⁻¹ can be obtained at a current density of 10 A g⁻¹ with a low capacitance loss of only 0.8% after 3000 cycles. This enhanced performance is attributed to the porous and hierarchical structures of the NiCoO₂ nanosheets nanotubes, which can offer more contact area between active materials and the electrolyte ions, buffer the large volume change during the fast charging/discharging process simultaneously. Furthermore, the entirely open ends of the NiCoO₂ nanosheets nanotubes provide additional paths for electrolyte.

Acknowledgments

This research was supported partially by the National Natural Science Foundation of China (No. 51273158, 21303131); Natural Science Basis Research Plan in Shaanxi Province of China (No. 2012JQ6003, 2013KJXX-49); Ph.D. Programs Foundation of Ministry of Education of China (No. 20120201120048); Program for New Century Excellent Talents in University (NCET-13-0449). The authors are grateful to the Fundamental Research Funds for the Central Universities (xjj2012092) for financial support and thank Prof. Chunming Niu for the valuable suggestions.

Appendix A. Supplementary data

Supplementary data related to this article can be found at <http://dx.doi.org/10.1016/j.jpowsour.2014.05.077>.

References

- [1] A.S. Arico, P. Bruce, B. Scrosati, J.M. Tarascon, W. Van, *Nat. Mater.* 4 (2005) 366.
- [2] J.R. Miller, P. Simon, *Science* 321 (2008) 651.
- [3] P. Simon, Y. Gogotsi, *Nat. Mater.* 7 (2008) 845.
- [4] C. Peng, S.W. Zhang, X.H. Zhou, G.Z. Chen, *Energy Environ. Sci.* 3 (2010) 1499.
- [5] G.P. Wang, L. Zhang, J.J. Zhang, *Chem. Soc. Rev.* 41 (2012) 797.
- [6] H.L. Wang, H.S. Casalongue, Y.Y. Liang, H.J. Dai, *J. Am. Chem. Soc.* 132 (2010) 7472.
- [7] C.Z. Yuan, L. Yang, L.R. Hou, L.F. Shen, X.G. Zhang, X.W. Lou, *Energy Environ. Sci.* 5 (2012) 7883.
- [8] W. Chen, R.B. Rakhi, L.B. Hu, X. Xie, Y. Cui, H.N. Alshareef, *Nano Lett.* 11 (2011) 5165.
- [9] E. Kim, D. Son, T.G. Kim, J. Cho, B. Park, K.S. Ryu, S.H. Chan, *Angew. Chem. Int. Ed.* 43 (2004) 5987.
- [10] G.X. Wang, H. Liu, J. Liu, S.Z. Qiao, G.Q.M. Lu, P. Munroe, H. Ahn, *Adv. Mater.* 22 (2010) 4944.
- [11] D. Mao, J. Yao, X. Lai, M. Yang, J. Du, D. Wang, *Small* 7 (2011) 578.
- [12] X.W. Lou, C.M. Li, L.A. Archer, *Adv. Mater.* 21 (2009) 2536.
- [13] G.Q. Zhang, X.W. Lou, *Adv. Mater.* 25 (2013) 976.
- [14] F. Cheng, J. Shen, B. Peng, Y. Pan, Z. Tao, J. Chen, *Nat. Chem.* 3 (2011) 79.
- [15] L. Zhou, D. Zhao, X.W. Lou, *Adv. Mater.* 24 (2012) 745.
- [16] T.Y. Wei, C.H. Chen, H.C. Chien, S.Y. Lu, C.C. Hu, *Adv. Mater.* 22 (2010) 347.
- [17] H. Jiang, J. Ma, C.Z. Li, *Chem. Commun.* 48 (2012) 4465.
- [18] H.L. Wang, Q.M. Gao, L. Jiang, *Small* 7 (2011) 2454.
- [19] G.Q. Zhang, H.B. Wu, H.E. Hoster, M.B. Chan-park, X.W. Lou, *Energy Environ. Sci.* 5 (2012) 9453.
- [20] C.Z. Yuan, J.Y. Li, L.R. Hou, L. Yang, L.F. Shen, X.G. Zhang, *J. Mater. Chem.* 22 (2012) 16084.
- [21] L.L. Li, Y.L. Cheah, Y. Ko, P. Teh, G. Wee, C.L. Wong, S.J. Peng, M. Srinivasan, *J. Mater. Chem. A* 1 (2013) 10935.
- [22] J.W. Xiao, S.H. Yang, *J. Mater. Chem.* 22 (2012) 12253.
- [23] W. Ni, F. Liang, J. Liu, X. Qu, C. Zhang, J. Li, Q. Wang, Z. Yang, *Chem. Commun.* 47 (2011) 4727.
- [24] X. Xu, J. Liang, H. Zhou, D.M. Lv, F.X. Liang, Z.L. Yang, S.J. Ding, D.M. Yu, *J. Mater. Chem. A* 1 (2013) 2995.
- [25] X. Xu, G.R. Yang, J. Liang, S.J. Ding, C.L. Tang, H.H. Yang, W. Yan, G.D. Yang, D.M. Yu, *J. Mater. Chem. A* 2 (2014) 116.
- [26] X. Xu, Z.Y. Fan, S.J. Ding, D.M. Yu, Y.P. Du, *Nanoscale* 6 (2014) 5245.
- [27] J. Liang, B.T. Dong, S.J. Ding, C.P. Li, B.Q. Li, J. Li, G. Yang, *J. Mater. Chem. A*, <http://dx.doi.org/10.1039/b802067c>.

- [28] H.B. Wu, H. Pang, X.W. Lou, *Energy Environ. Sci.* 6 (2013) 3619.
- [29] G.Q. Zhang, X.W. Lou, *Sci. Rep.* 3 (2013) 1470.
- [30] X. Wang, X.D. Han, M.F. Lim, N.D. Singh, C.L. Gan, M. Jan, P.S. Lee, *J. Phys. Chem. C* 116 (2012) 12448.
- [31] H.W. Wang, Z.A. Hu, Y.Q. Chang, Y.L. Chen, H.Y. Wu, Z.Y. Zhang, Y.Y. Yang, *J. Mater. Chem.* 21 (2011) 10504.
- [32] X.Y. Liu, S.J. Shi, Q.Q. Xiong, L. Li, Y.J. Zhang, H. Tang, C.D. Gu, X.L. Wang, J.P. Tu, *ACS Appl. Mater. Interfaces* 5 (2013) 8790.
- [33] X.Y. Liu, Y.Q. Zhang, X.H. Xia, S.J. Shi, Y. Lu, X.L. Wang, C.D. Gu, J.P. Tu, *J. Power Sources* 247 (2014) 178.
- [34] X. Xu, J. Liang, H. Zhou, S.J. Ding, D.M. Yu, *RSC Adv.* 4 (2014) 3181.